nature medicine

Therapy of Pelizaeus-Merzbacher disease in mice by feeding a cholesterol-enriched diet

Gesine Saher[1], Fabian Rudolphi[1,3], Kristina Corthals[1,3], Torben Ruhwedel[1], Karl-Friedrich Schmidt[2], Siegrid Löwel[2], Payam Dibaj[1], Benoit Barrette[1], Wiebke Möbius[1] & Klaus-Armin Nave[1]

Duplication of *PLP1* (proteolipid protein gene 1) and the subsequent overexpression of the myelin protein PLP (also known as DM20) in oligodendrocytes is the most frequent cause of Pelizaeus-Merzbacher disease (PMD), a fatal leukodystrophy[1] without therapeutic options[2,3]. PLP binds cholesterol and is contained within membrane lipid raft microdomains[4]. Cholesterol availability is the rate-limiting factor of central nervous system myelin synthesis[5]. Transgenic mice with extra copies of the *Plp1* gene[6] are accurate models of PMD. Dysmyelination[6–8] followed by demyelination[9,10], secondary inflammation and axon damage contribute to the severe motor impairment in these mice[9,10]. The finding that in *Plp1*-transgenic oligodendrocytes, PLP and cholesterol accumulate in late endosomes and lysosomes (endo/lysosomes)[9,11–13], prompted us to further investigate the role of cholesterol in PMD. Here we show that cholesterol itself promotes normal PLP trafficking and that dietary cholesterol influences PMD pathology. In a preclinical trial, PMD mice were fed a cholesterol-enriched diet. This restored oligodendrocyte numbers and ameliorated intracellular PLP accumulation. Moreover, myelin content increased, inflammation and gliosis were reduced and motor defects improved. Even after onset of clinical symptoms, cholesterol treatment prevented disease progression. Dietary cholesterol did not reduce *Plp1* overexpression but facilitated incorporation of PLP into myelin membranes. These findings may have implications for therapeutic interventions in patients with PMD.

We have previously shown that mouse mutants lacking cholesterol synthesis in oligodendrocytes (*Fdft1*$^{flox/flox}$ × *Cnp1*$^{+/cre}$, termed cSQS knockout) express myelin protein genes, including *Plp1*, at a low level[5]. We therefore tested the potential application of an inhibitor of squalene synthase and cholesterol synthesis (squalestatin) for the downregulation of toxic *Plp1* overexpression in mice with increased *Plp1* gene dosage[6] (PLP-tg$^{72/72}$, *Plp1* transgenic line 72 containing three copies of the transgene, termed PMD mice hereafter, **Supplementary Table 1**). To protect PMD mice from the possible side effects of high-dose squalestatin treatment, we supplemented peripheral cholesterol levels with a high-cholesterol diet. We assumed that the CNS was shielded from cholesterol from the circulation by the blood-brain barrier (BBB)[14]. To our surprise, all mice of this pilot trial improved dramatically in comparison to the known PMD phenotype in mice (data not shown). This raised the possibility that the increase in circulating cholesterol by itself (or an indirect effect) ameliorates the leukodystrophy associated with PLP overexpression.

Next, we systematically compared PMD mice that received a cholesterol-enriched diet with littermates receiving normal chow. Serum cholesterol levels of PMD mice before treatment were not different from those of wild-type (WT) mice and increased in response to the cholesterol-enriched chow by about 10% as expected[15]. The cholesterol-rich diet had no effect on body weight (**Supplementary Fig. 1**).

In PMD mice injected with Evans blue dye (0.5 µg per g body weight intraperitoneally) to test the permeability of the BBB, the BBB was compromised already at 2 weeks of age (**Supplementary Fig. 2a**). Mice with a lower level of *Plp1* overexpression (PLP-tg$^{+/66}$, *Plp1* transgenic line 66 containing seven copies of the transgene)[6] lack such BBB opening (data not shown), in line with other studies[8,16]. In addition, cSQS knockout mouse mutants show normal BBB properties. On a cholesterol-enriched diet, cSQS mutant mice remain severely hypomyelinated[5]. Thus, we wanted to determine whether circulating cholesterol can cross the BBB in PMD mice. When tested 7 d after a single injection of BODIPY-cholesterol, fluorescence was readily detectable in the optic nerve from PMD mice (in contrast to WT controls) with a fiber-like pattern typical for myelinated axons (**Fig. 1a** and **Supplementary Fig. 2b**). Thus, in PMD mice peripheral cholesterol can pass the BBB, which is possibly perturbed by secondary inflammation[9,17].

Next, we wanted to determine whether dietary cholesterol supplementation can ameliorate existing pathology in PMD mice. We tested PMD mice (n = 15 or 16) that were put on a high-cholesterol diet at 6 weeks of age for a duration of 6 weeks, that is, after the onset of clinical signs as measured by decreased visual acuity (**Fig. 1b**,**c**). Visual acuity further declined in untreated PMD mice, whereas in PMD mice receiving cholesterol, visual acuity remained stable (**Fig. 1c** and **Supplementary Fig. 3**). PLP overexpression in PMD oligodendrocytes

[1]Department of Neurogenetics, Max Planck Institute of Experimental Medicine, Göttingen, Germany. [2]Bernstein Focus Neurotechnology and Johann-Friedrich-Blumenbach Institute of Zoology and Anthropology, Georg-August University, Göttingen, Germany. [3]These authors contributed equally to this work. Correspondence should be addressed to G.S. (saher@em.mpg.de) or K.-A.N. (nave@em.mpg.de).

Received 22 November 2011; accepted 15 May 2012; published online 17 June 2012; doi:10.1038/nm.2833

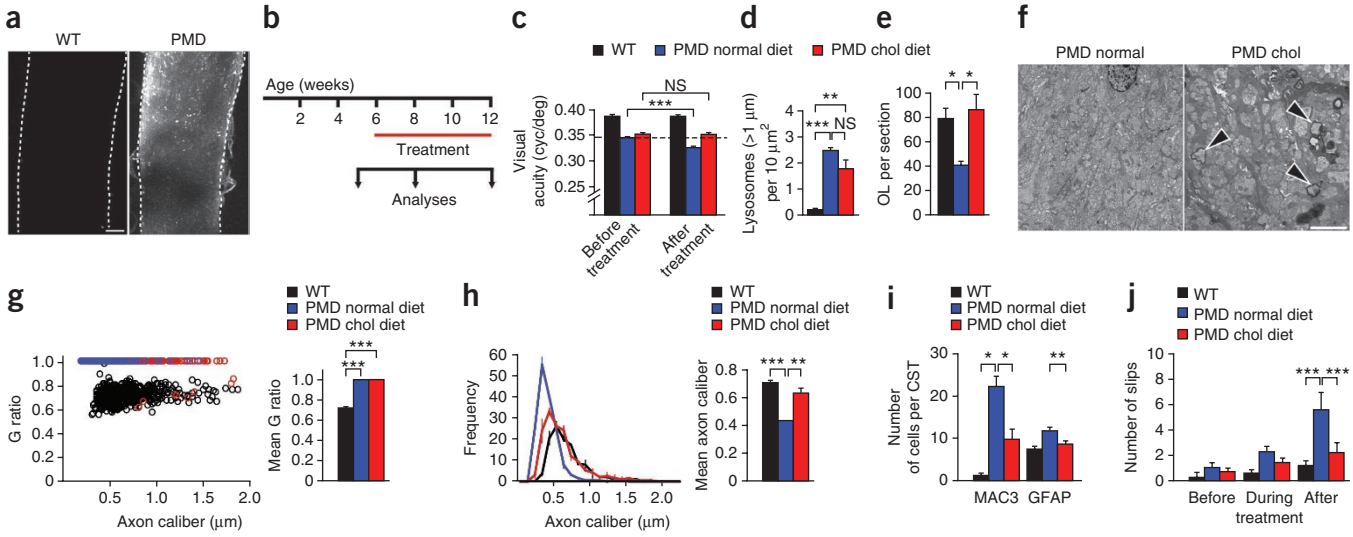

Figure 1 Cholesterol prevents the clinical deterioration of PMD mice. (**a**) BODIPY-cholesterol–derived fluorescence in the optic nerve of WT mice and PMD mice 7 d after intraperitoneal (i.p.) injection, as analyzed by two-photon microscopy. Scale bar, 50 µm. (**b**) Treatment scheme. PMD mice were given normal chow (control group) or cholesterol-enriched chow (treatment group) starting at 6 weeks of age with a 6-week duration. (**c**) Behavioral analysis using a virtual-reality optomotor system ($n = 9$ or 10). The dashed line marks the level of PMD mice on normal diet before treatment (cyc/deg, cycles per degree). (**d**) Quantification of large lysosomes (>1 µm in diameter) in the optic nerve ($n = 3$). (**e**) Number of oligodendrocytes (OL) per optic nerve cross section ($n = 3$). (**f**) Ultrastructural analysis of optic nerves revealing myelinated axons (arrowheads) in PMD mice on high-cholesterol diet (scale bar, 5 µm). (**g**) G-ratio analysis of optic nerve axons from WT and PMD mice ($n = 3$). (**h**) Axon caliber measurement of axon diameters of WT, PMD and cholesterol-fed PMD mice ($n = 3$). (**i**) Quantification of MAC3-positive microglia and GFAP-positive astrocytes in the corticospinal tract (CST) ($n = 3$–5 mice). (**j**) Beam tests, measuring the number of slips before the onset of treatment, after 3 weeks (during) and at the end of the trial (after) ($n = 9$ or 10 mice). Data are means ± s.e.m. $^*P < 0.05$; $^{**}P < 0.01$; $^{***}P < 0.001$, one-way (**d**–**i**) or two-way (**c**,**j**) analysis of variance (ANOVA) followed by Bonferroni test.

resulted in its accumulation in the Lamp1-positive endo/lysosomal compartment (**Supplementary Fig. 4**) in agreement with previous studies[11–13]. The high-cholesterol diet slightly decreased the abundance of large lysosomes (**Fig. 1d**). The number of oligodendrocytes, which is reduced in PMD optic nerves to about 50% of that in WT mice, was normalized (**Fig. 1e**), although improvement in myelination was only minimal (**Fig. 1f**,**g**). Notably, axon calibers in PMD mice increased to WT sizes after cholesterol treatment (**Fig. 1h**). Axonal loss was not observed in treated or untreated PMD mice at the end of this study (data not shown), in agreement with another study[9]. Secondary astrogliosis and microgliosis in the spinal cord were reduced by dietary cholesterol (**Fig. 1i**). This 6-week-long cholesterol treatment delayed the decline in motor coordination typically observed in PMD mice (**Fig. 1j**). Thus, despite persistent hypomyelination, cholesterol administration prevents the clinical deterioration in PMD mice, potentially by maintaining oligodendrocyte numbers, increasing axon calibers and

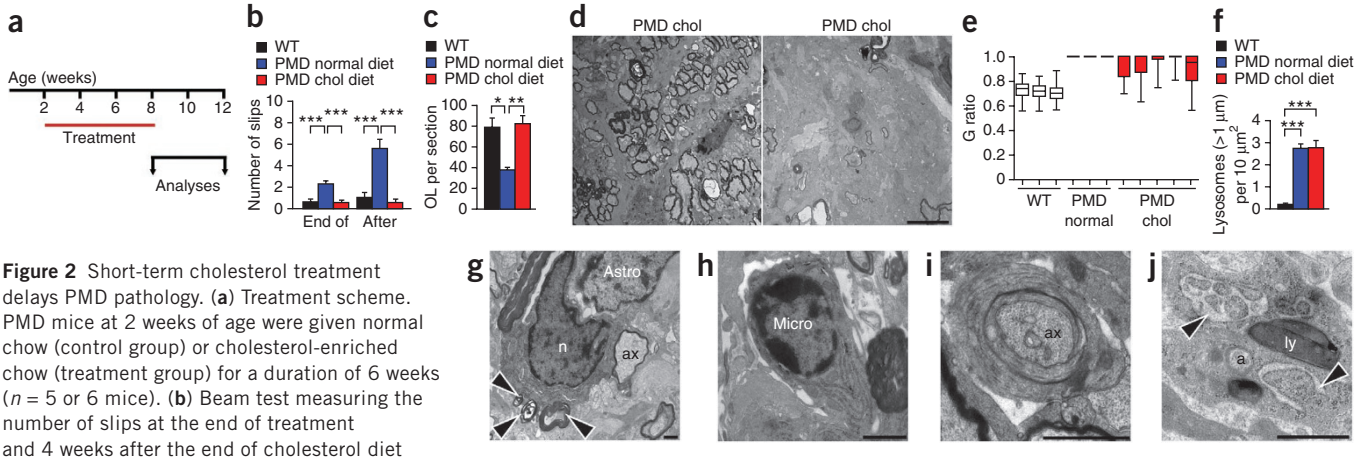

Figure 2 Short-term cholesterol treatment delays PMD pathology. (**a**) Treatment scheme. PMD mice at 2 weeks of age were given normal chow (control group) or cholesterol-enriched chow (treatment group) for a duration of 6 weeks ($n = 5$ or 6 mice). (**b**) Beam test measuring the number of slips at the end of treatment and 4 weeks after the end of cholesterol diet ($n = 5$–7 mice). (**c**) Number of oligodendrocytes per optic nerve cross-section from WT and PMD mice ($n = 3$–6). (**d**) Electron microscopic images of the optic nerve from two different PMD mice in the cholesterol group showing variability of myelination (scale bar, 5 µm). (**e**) Boxplot analysis of g-ratios of individual mice reflecting the variability of treatment benefit in PMD mice. (**f**) Quantification of lysosomes (>1 µm in diameter) in the optic nerve of WT and PMD mice ($n = 3$). (**g**–**j**) Electron microscopic images of optic nerves of cholesterol treated PMD mice show signs of ongoing pathology (**g**), such as oligodendrocytes (n, oligodendrocyte nucleus) with degenerating myelin profiles marked by arrowheads and a thin myelin sheath surrounding an axon (ax) (Astro, astrocyte), as well as microglia (Micro) with characteristic undulating long ER cisternae (**h**) and remyelinating profiles (**i**). (**j**) Oligodendrocytes containing dilated ER (a, autophagosome; ly, lysosome; scale bars, 1 µm). Data are means ± s.e.m. $^*P < 0.05$; $^{**}P < 0.01$; $^{***}P < 0.001$, one-way (**c**,**f**) or two-way (**b**) ANOVA followed by Bonferroni test.

reducing gliosis. The observation that not all defects were reverted may be due in part to the late onset and brevity of the treatment.

Next, we tested whether a similar treatment of PMD mice around the peak of myelination would be therapeutically more efficient (treatment from 2–8 weeks of age, analysis at 12 weeks of age) (**Fig. 2a**). In this treatment paradigm, motor performance did not overtly decline during the 4 weeks after cholesterol supplementation (**Fig. 2b**). Oligodendrocyte numbers were maintained (**Fig. 2c**). Ultrastructural analysis revealed a considerable number of myelinated axons; however, there was substantial interindividual variability (**Fig. 2d**,**e**). Large lysosomes were as frequent as in untreated PMD mice (**Fig. 2f**). Degenerating myelin profiles indicated ongoing demyelination, and signs of remyelination were also observed (**Fig. 2g–i**). Dilated endoplasmic reticulum (ER) was prominent in oligodendrocytes of untreated PMD mice, pointing to alterations also in this cellular compartment (**Fig. 2j** and see below). Thus, cholesterol treatment over the peak myelination period is advantageous.

Finally, we tested a combination of both early-onset and long-term treatment with cholesterol (2–12 weeks of age; n = 7–9; **Fig. 3a**). A high-cholesterol diet markedly increased the diameter of PMD optic nerves and normalized myelin content to near WT levels (**Fig. 3b–d**). Oligodendrocyte numbers and axon calibers also normalized (**Fig. 3e**,**f**). A high-cholesterol diet visibly reduced PLP abundance in the endo/lysosomal compartment and decreased the number of large lysosomes in PMD oligodendrocytes (**Fig. 3g**,**h** and **Supplementary Fig. 5**). Theoretically, *Plp1* overexpression and increased availability of cholesterol could elevate the amount of PLP in myelin membranes. However, by western blot analysis the amount of PLP in myelin purified from PMD mice was the same as in WT mice, irrespective of the diet (**Fig. 3i**). In the PMD spinal cord, the high-cholesterol diet normalized myelination and reduced reactive gliosis and T cell infiltration (**Supplementary Fig. 6**). All these changes correlated with an amelioration of the clinical score and improved the motor abilities of PMD mice close to WT levels (**Fig. 3j** and **Supplementary Video 1**). Already at 6 weeks of age, visual acuity was almost normal (data not shown). Unexpectedly, when PMD mice started the high-cholesterol diet only 1 week later (3–12 weeks, n = 8), visual acuity was comparable to that of PMD mice on a high-cholesterol diet from 6 to 12 weeks (**Fig. 1c**), and optic nerves were poorly myelinated. These findings underscore that the third week of life is crucial for myelination in the optic nerve of PMD mice. We note that at the age of 6 months PMD mice on a high-cholesterol diet appear healthy (n = 14, data not shown). Taken together, our results suggest that, for maximal amelioration of PMD pathology, treatment should begin early in life and continue into adulthood.

Oligodendrocyte-specific inactivation of cholesterol synthesis in *Plp1*-transgenic mice (cSQS knockout × PLP-tg$^{+/66}$) further aggravates pathology (**Supplementary Fig. 7** and **Supplementary Video 2**). We therefore asked whether cholesterol synthesis itself is affected in PMD oligodendrocytes and compared the expression of sterol-synthesizing enzymes by real-time RT-PCR in spinal cord from WT and PMD mice. The expression of *Hmgcr* (encoding the rate-limiting enzyme of cholesterol biosynthesis) and of *Fdft1* was strongly reduced in PMD mice on a normal diet as compared to WT mice (**Fig. 4a**). Notably, in brains of Niemann-Pick type C1 (NPC1) model mice, cholesterol synthesis is also downregulated[18,19]. PMD oligodendrocytes also have reduced expression of myelin genes as compared to WT mice[6,12]. We found reduced expression of *Mbp* (encoding myelin basic protein) in PMD spinal cord compared to WT spinal cord (for *Plp1*, this reduction is leveled out by the higher gene dosage), but no obvious oligodendrocyte loss (**Fig. 4a** and **Supplementary Fig. 6**). In cholesterol-fed PMD mice, we observed

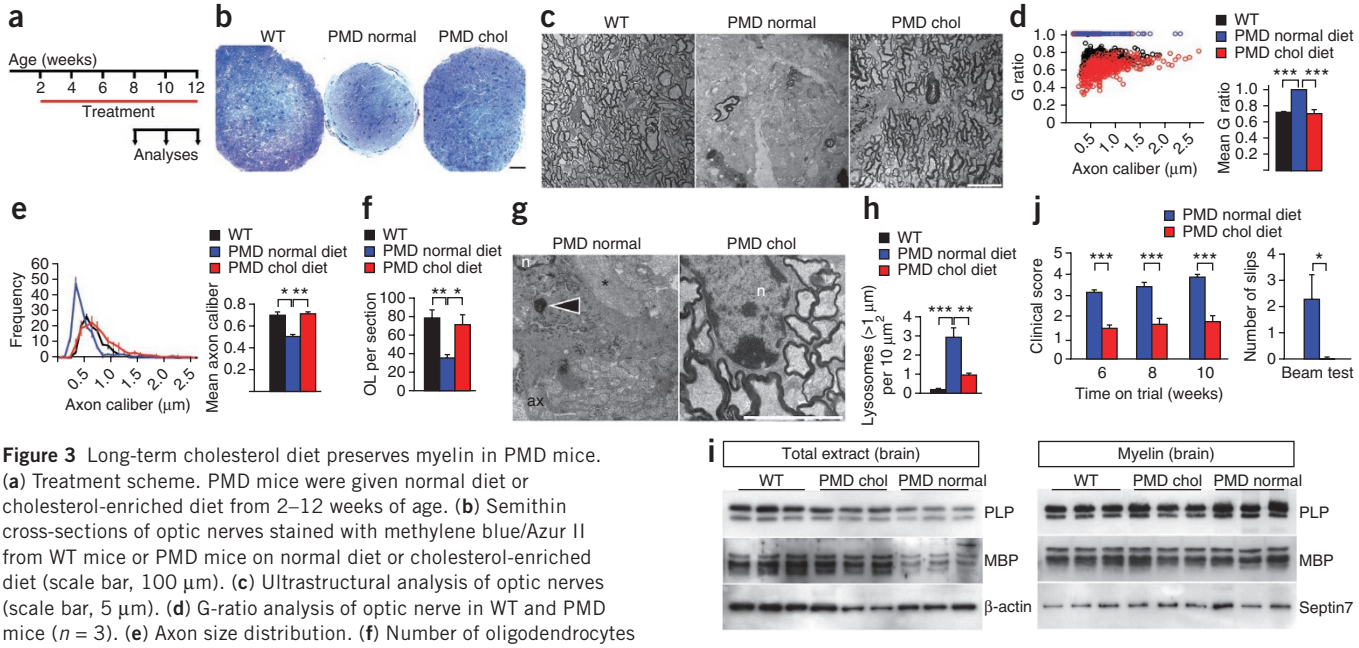

Figure 3 Long-term cholesterol diet preserves myelin in PMD mice. (**a**) Treatment scheme. PMD mice were given normal diet or cholesterol-enriched diet from 2–12 weeks of age. (**b**) Semithin cross-sections of optic nerves stained with methylene blue/Azur II from WT mice or PMD mice on normal diet or cholesterol-enriched diet (scale bar, 100 μm). (**c**) Ultrastructural analysis of optic nerves (scale bar, 5 μm). (**d**) G-ratio analysis of optic nerve in WT and PMD mice (n = 3). (**e**) Axon size distribution. (**f**) Number of oligodendrocytes per optic nerve cross section (n = 3). (**g**) Ultrastructural analysis of optic nerves from PMD mice. The arrowhead shows a lysosome (scale bar, 1 μm; ax, axon; n, nucleus, *, astrocyte process). (**h**) Quantification showing the abundance of large lysosomes in optic nerve (>1 μm in diameter; n = 3). (**i**) Western blot analysis of brain extracts and myelin-enriched fractions detecting the compact myelin proteins PLP and MBP. Loading controls are β-actin in extracts and Septin7 in myelin fractions. (**j**) Evaluation of the clinical score in mice. 1, normal; 2, mild tremor, mild ataxia; 3, strong tremor, strong ataxia; 4, seizures; 5, death (n = 7–9; unpaired Mann-Whitney test). Motor abilities of PMD mice after therapy assessed with a beam test (Student's t test, n = 7–9). Data are means ± s.e.m. $^*P < 0.05$; $^{**}P < 0.01$; $^{***}P < 0.001$, one-way ANOVA followed by Bonferroni test (**d**–**f**,**h**,**j**).

increased expression of *Mbp* and *Plp1* (**Fig. 4a**), probably reflecting ongoing myelination (compare to **Supplementary Fig. 6**). Thus, cholesterol treatment of PMD mice does not reduce *Plp1* overexpression, the primary cause of disease. Unexpectedly, cholesterol also increased transcription of genes for sterol-synthesizing enzymes (**Fig. 4a**). This finding was unexpected because it is thought that external cholesterol negatively feeds back on endogenous cholesterol biosynthesis[20] (see below).

To obtain insight into the mechanism by which additional cholesterol restores the integrity of *Plp1*-overexpressing oligodendrocytes, we cultured primary oligodendrocytes from WT and PMD mice (PMD oligodendrocytes). During differentiation, we supplemented the medium with cholesterol or zaragozic acid A , an inhibitor of squalene synthase and cholesterol biosynthesis (**Fig. 4b–h**). Compared to WT oligodendrocytes, PMD oligodendrocytes more often accumulated PLP in the cell soma, colocalizing with Lamp1 in endo/lysosomes. The addition of cholesterol decreased this intracellular PLP retention to the same level as found in WT oligodendrocytes (**Fig. 4c**).

Cholesterol promotes the differentiation of Schwann cells[21]. We found that cholesterol supplementation slightly enhanced the maturation of WT oligodendrocytes when we scored PLP-positive membrane sheaths (**Fig. 4d**). In turn, the inhibition of cholesterol synthesis reduced oligodendrocyte maturation by about 50% (**Fig. 4e**). Cholesterol availability may thus be limiting for the maturation of oligodendrocytes. In cultures of PMD oligodendrocytes, only 40% of cells matured compared to WT oligodendrocytes. This maturation almost doubled in the presence of extra cholesterol (**Fig. 4d**). Notably, the poor maturation of PMD oligodendrocytes was not further

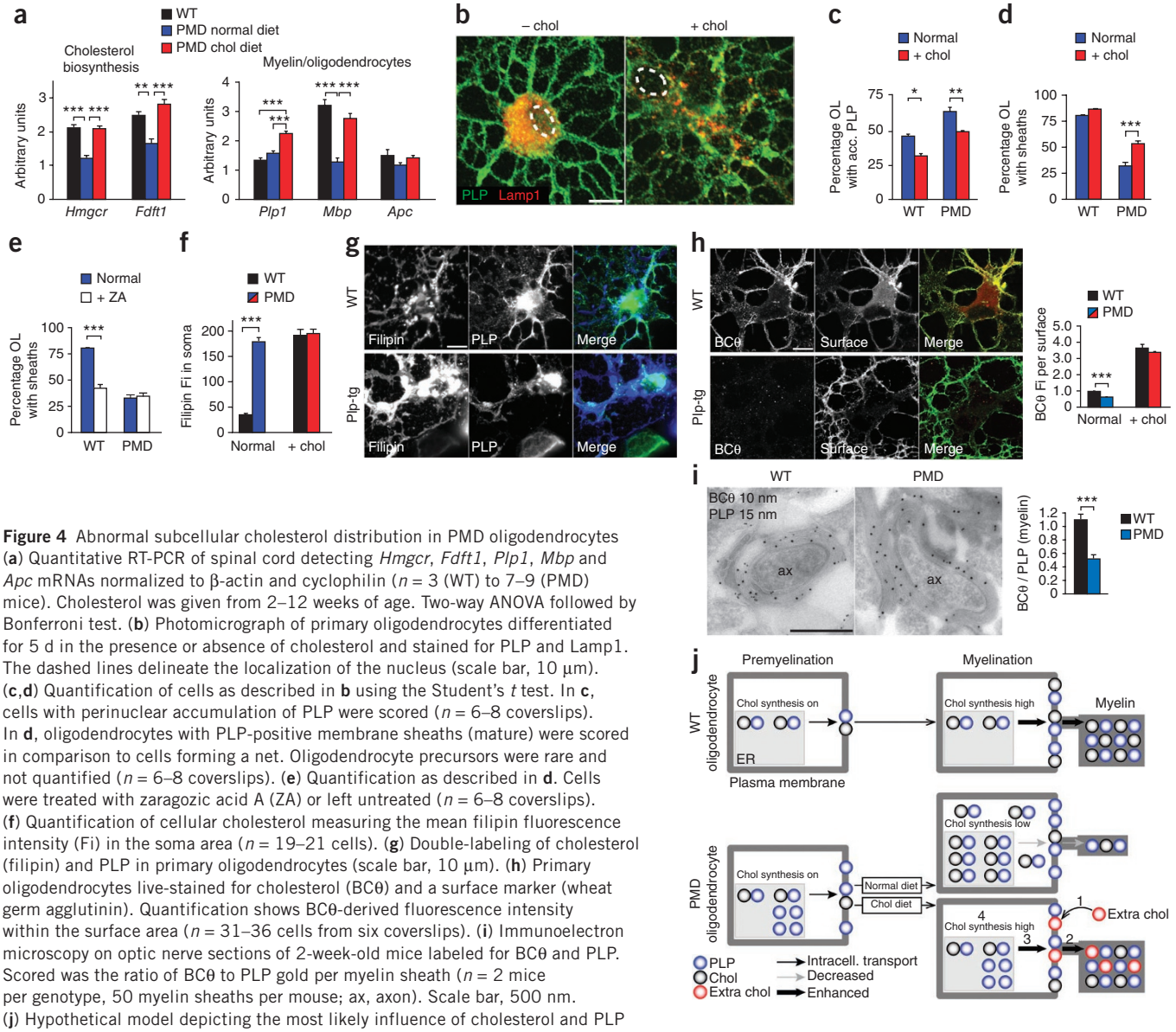

Figure 4 Abnormal subcellular cholesterol distribution in PMD oligodendrocytes (**a**) Quantitative RT-PCR of spinal cord detecting *Hmgcr*, *Fdft1*, *Plp1*, *Mbp* and *Apc* mRNAs normalized to β-actin and cyclophilin ($n = 3$ (WT) to 7–9 (PMD) mice). Cholesterol was given from 2–12 weeks of age. Two-way ANOVA followed by Bonferroni test. (**b**) Photomicrograph of primary oligodendrocytes differentiated for 5 d in the presence or absence of cholesterol and stained for PLP and Lamp1. The dashed lines delineate the localization of the nucleus (scale bar, 10 µm). (**c**,**d**) Quantification of cells as described in **b** using the Student's *t* test. In **c**, cells with perinuclear accumulation of PLP were scored ($n = 6–8$ coverslips). In **d**, oligodendrocytes with PLP-positive membrane sheaths (mature) were scored in comparison to cells forming a net. Oligodendrocyte precursors were rare and not quantified ($n = 6–8$ coverslips). (**e**) Quantification as described in **d**. Cells were treated with zaragozic acid A (ZA) or left untreated ($n = 6–8$ coverslips). (**f**) Quantification of cellular cholesterol measuring the mean filipin fluorescence intensity (Fi) in the soma area ($n = 19–21$ cells). (**g**) Double-labeling of cholesterol (filipin) and PLP in primary oligodendrocytes (scale bar, 10 µm). (**h**) Primary oligodendrocytes live-stained for cholesterol (BCθ) and a surface marker (wheat germ agglutinin). Quantification shows BCθ-derived fluorescence intensity within the surface area ($n = 31–36$ cells from six coverslips). (**i**) Immunoelectron microscopy on optic nerve sections of 2-week-old mice labeled for BCθ and PLP. Scored was the ratio of BCθ to PLP gold per myelin sheath ($n = 2$ mice per genotype, 50 myelin sheaths per mouse; ax, axon). Scale bar, 500 nm. (**j**) Hypothetical model depicting the most likely influence of cholesterol and PLP on PMD pathology. In WT oligodendrocytes, PLP binds cholesterol at a certain ratio that is required for myelin assembly. In untreated PMD oligodendrocytes, overexpressed PLP leads to the intracellular enrichment of cholesterol. In the cytoplasm, elevated cholesterol impairs intracellular trafficking. Consequently, the cholesterol content in the plasma membrane is reduced, which diminishes myelin assembly. Elevated cholesterol in the ER downregulates cholesterol synthesis. In treated PMD mice, the extra cholesterol improves the ratio of PLP to cholesterol in the plasma membrane (1) and promotes the assembly of myelin membranes (2). This reduces the intracellular cholesterol concentration (3), which in turn induces cholesterol synthesis (4). Data are means ± s.e.m. $*P < 0.05$; $**P < 0.01$; $***P < 0.001$, one-way ANOVA followed by Bonferroni test (**a**,**c**–**f**,**h**,**i**).

impaired by zaragozic acid A (**Fig. 4e**). This underscores that cholesterol synthesis is perturbed in PMD oligodendrocytes, correlating with our *in vivo* data.

What causes the downregulation of cholesterol synthesis? PMD oligodendrocytes, grown in normal medium and labeled for cholesterol (using filipin, a fluorescent antibiotic that binds unesterified cholesterol), appeared cholesterol laden (**Fig. 4f,g**). Mean filipin-derived fluorescence intensity, which correlates with the cholesterol content[22], could barely be increased by cholesterol supplementation, in contrast to a six- to sevenfold increase seen in WT oligodendrocytes. Moreover, filipin fluorescence was barely seen in the soma of WT oligodendrocytes. In PMD oligodendrocytes, the strong intracellular filipin fluorescence was also found outside of endo/lysosomes (**Supplementary Fig. 8a**). When optic nerve sections from PMD mice at 2 weeks of age were stained for BCθ (ref. 23), a bacterial toxin that binds cholesterol, the ER of oligodendrocytes from PMD mice contained noticeably more BCθ-derived label compared to WT controls (**Supplementary Fig. 8b**). Thus, in the active phase of the disease, cholesterol abundance is increased in the ER, the cellular compartment that controls cellular cholesterol synthesis[20]. It is therefore plausible that cholesterol-laden PMD oligodendrocytes have downregulated cholesterol synthesis.

In what way could an elevated content of intracellular cholesterol affect myelin assembly? High cholesterol impairs intracellular trafficking[24–27]. PLP overexpression in BHK cells prevents plasma membrane trafficking of a membrane lipid raft marker[13], possibly by elevation of intracellular cholesterol. In NPC1-null cells, the cholesterol content in the plasma membrane is decreased[28]. Thus, PMD oligodendrocytes may also suffer from intracellular trafficking defects and from reduced cholesterol content in the plasma membrane. Indeed, the plasma membrane of PMD oligodendrocytes showed reduced staining with BCθ to about 60% of WT levels (**Fig. 4h**). Moreover, the ratio of BCθ to PLP (quantified by immunoelectron microscopy) also revealed a similar reduction of cholesterol in myelin sheaths of PMD optic nerves (**Fig. 4i**). Notably, the staining density of PLP was similar in mutants and controls, in agreement with our biochemical data (**Fig. 3i**). The reduced association of PLP with membrane lipid rafts in PMD myelin further supports this notion[10].

Our data have revealed a previously unknown role of cholesterol in the clinical course of PMD (**Fig. 4j** contains a working model). PLP overexpression, when untreated, leads to increased intracellular concentration of this myelin protein and aberrant deposition in endo/lysosomes. As PLP associates with cholesterol, cholesterol abundance is also increased intracellularly. Elevated cholesterol in the ER seems to downregulate endogenous cholesterol synthesis. In the secretory pathways, excess cholesterol impairs vesicular transport. The resulting decreased amount of cholesterol in the plasma membrane seems too low for efficient myelin assembly[29]. We envision that the association of cholesterol with (increased) PLP in the ER inhibits PMD oligodendrocytes from downregulating cholesterol synthesis early enough to prevent the intracellular traffic jam that ultimately leads to impaired myelin assembly. This premature arrest of myelination in PMD mice[6–10] can be overcome by the administration of external cholesterol, presumably by improving the stoichiometry between PLP and cholesterol in the plasma membrane. Once bound to sufficient cholesterol, PLP is integrated into myelin membranes. This subsequently reduces the intracellular cholesterol and PLP concentration and allows for an increase of cell-autonomous cholesterol synthesis, which further promotes myelin membrane synthesis.

Together, our data suggest that dietary cholesterol does not cure PMD but has a striking potential to relieve oligodendrocytes from defects caused by Plp1 overexpression. This amelioration of disease in a mouse model of PMD has implications for therapeutic interventions in patients with PMD.

METHODS

Methods and any associated references are available in the online version of the paper.

Note: Supplementary information is available in the online version of the paper.

ACKNOWLEDGMENTS

We dedicate this work to the memory of Jim Garbern for his support of PMD research. We are grateful to A. Fahrenholz, T. Freerck, M. Schildmann, M. Matthes and A. Kanbach for technical support and thank J. Edgar for helpful comments on the manuscript. We thank M. Grebe (Umea University) for providing the BCθ expression construct and Pfizer for the generous gift of the squalestatin CP-340868. This work was funded by the PMD foundation and the Deutsche Forschungsgemeinschaft (SA2114/1-1) to G.S. K.-A.N. is supported by the EU-FP7 (Leukotreat, Ngidd), the Bundesministerium für Bildung und Forschung (BMBF; Leukonet) and a European Research Council (ERC) Advanced Grant. Support of the BMBF to S.L. and K.-F.S. is gratefully acknowledged (01GQ0810).

AUTHOR CONTRIBUTIONS

G.S. supervised the project, conducted experiments and wrote the manuscript; F.R., K.C. and T.R. conducted experiments, K.-F.S. and S.L. performed visual acuity measurements, P.D. conducted the two-photon microscopic analysis, B.B. implemented the beam test, W.M. supervised and contributed to electron microscopic studies, and K.-A.N. contributed to the discussion and the writing of the manuscript.

COMPETING FINANCIAL INTERESTS

The authors declare no competing financial interests.

Published online at http://www.nature.com/doifinder/10.1038/nm.2833.
Reprints and permissions information is available online at http://www.nature.com/reprints/index.html.

1. Seitelberger, F. Neuropathology and genetics of Pelizaeus-Merzbacher disease. *Brain Pathol.* **5**, 267–273 (1995).
2. Garbern, J.Y. Pelizaeus-Merzbacher disease: Genetic and cellular pathogenesis. *Cell Mol. Life Sci.* **64**, 50–65 (2007).
3. Woodward, K.J. The molecular and cellular defects underlying Pelizaeus-Merzbacher disease. *Expert Rev. Mol. Med.* **10**, e14 (2008).
4. Simons, M., Kramer, E.M., Thiele, C., Stoffel, W. & Trotter, J. Assembly of myelin by association of proteolipid protein with cholesterol- and galactosylceramide-rich membrane domains. *J. Cell Biol.* **151**, 143–154 (2000).
5. Saher, G. *et al.* High cholesterol level is essential for myelin membrane growth. *Nat. Neurosci.* **8**, 468–475 (2005).
6. Readhead, C., Schneider, A., Griffiths, I. & Nave, K.A. Premature arrest of myelin formation in transgenic mice with increased proteolipid protein gene dosage. *Neuron* **12**, 583–595 (1994).
7. Anderson, T.J. *et al.* Distinct phenotypes associated with increasing dosage of the PLP gene: implications for CMT1A due to PMP22 gene duplication. *Ann. NY Acad. Sci.* **883**, 234–246 (1999).
8. Anderson, T.J. *et al.* Late-onset neurodegeneration in mice with increased dosage of the proteolipid protein gene. *J. Comp. Neurol.* **394**, 506–519 (1998).
9. Edgar, J.M. *et al.* Demyelination and axonal preservation in a transgenic mouse model of Pelizaeus-Merzbacher disease. *EMBO Mol. Med.* **2**, 42–50 (2010).
10. Karim, S.A. *et al.* PLP/DM20 expression and turnover in a transgenic mouse model of Pelizaeus-Merzbacher disease. *Glia* **58**, 1727–1738 (2010).
11. Krämer, E.M., Schardt, A. & Nave, K.A. Membrane traffic in myelinating oligodendrocytes. *Microsc. Res. Tech.* **52**, 656–671 (2001).
12. Karim, S.A. *et al.* PLP overexpression perturbs myelin protein composition and myelination in a mouse model of Pelizaeus-Merzbacher disease. *Glia* **55**, 341–351 (2007).
13. Simons, M. *et al.* Overexpression of the myelin proteolipid protein leads to accumulation of cholesterol and proteolipid protein in endosomes/lysosomes: implications for Pelizaeus-Merzbacher disease. *J. Cell Biol.* **157**, 327–336 (2002).
14. Björkhem, I. & Meaney, S. Brain cholesterol: long secret life behind a barrier. *Arterioscler. Thromb. Vasc. Biol.* **24**, 806–815 (2004).
15. Alberti, S. *et al.* Hepatic cholesterol metabolism and resistance to dietary cholesterol in LXRbeta-deficient mice. *J. Clin. Invest.* **107**, 565–573 (2001).

16. Ip, C.W. *et al.* Origin of CD11b^{+} macrophage-like cells in the CNS of PLP-overexpressing mice: low influx of haematogenous macrophages and unchanged blood-brain-barrier in the optic nerve. *Mol. Cell Neurosci.* **38**, 489–494 (2008).
17. Stolp, H.B. & Dziegielewska, K.M. Review: Role of developmental inflammation and blood-brain barrier dysfunction in neurodevelopmental and neurodegenerative diseases. *Neuropathol. Appl. Neurobiol.* **35**, 132–146 (2009).
18. Xie, C., Lund, E.G., Turley, S.D., Russell, D.W. & Dietschy, J.M. Quantitation of two pathways for cholesterol excretion from the brain in normal mice and mice with neurodegeneration. *J. Lipid Res.* **44**, 1780–1789 (2003).
19. Liu, B. *et al.* Reversal of defective lysosomal transport in NPC disease ameliorates liver dysfunction and neurodegeneration in the *Npc1*$^{-/-}$ mouse. *Proc. Natl. Acad. Sci. USA* **106**, 2377–2382 (2009).
20. Brown, M.S. & Goldstein, J.L. The SREBP pathway: regulation of cholesterol metabolism by proteolysis of a membrane-bound transcription factor. *Cell* **89**, 331–340 (1997).
21. Saher, G. *et al.* Cholesterol regulates the endoplasmic reticulum exit of the major membrane protein P0 required for peripheral myelin compaction. *J. Neurosci.* **29**, 6094–6104 (2009).
22. Qin, C., Nagao, T., Grosheva, I., Maxfield, F.R. & Pierini, L.M. Elevated plasma membrane cholesterol content alters macrophage signaling and function. *Arterioscler. Thromb. Vasc. Biol.* **26**, 372–378 (2006).
23. Shepard, L.A. *et al.* Identification of a membrane-spanning domain of the thiol-activated pore-forming toxin Clostridium perfringens perfringolysin O: an α-helical to β-sheet transition identified by fluorescence spectroscopy. *Biochemistry* **37**, 14563–14574 (1998).
24. Karten, B., Peake, K.B. & Vance, J.E. Mechanisms and consequences of impaired lipid trafficking in Niemann-Pick type C1–deficient mammalian cells. *Biochim. Biophys. Acta* **1791**, 659–670 (2009).
25. Otomo, T., Higaki, K., Nanba, E., Ozono, K. & Sakai, N. Lysosomal storage causes cellular dysfunction in mucolipidosis II skin fibroblasts. *J. Biol. Chem.* **286**, 35283–35290 (2011).
26. Tang, Y., Leao, I.C., Coleman, E.M., Broughton, R.S. & Hildreth, J.E. Deficiency of niemann-pick type C-1 protein impairs release of human immunodeficiency virus type 1 and results in Gag accumulation in late endosomal/lysosomal compartments. *J. Virol.* **83**, 7982–7995 (2009).
27. Sobo, K. *et al.* Late endosomal cholesterol accumulation leads to impaired intra-endosomal trafficking. *PLoS ONE* **2**, e851 (2007).
28. Hawes, C.M., Wiemer, H., Krueger, S.R. & Karten, B. Pre-synaptic defects of NPC1-deficient hippocampal neurons are not directly related to plasma membrane cholesterol. *J. Neurochem.* **114**, 311–322 (2010).
29. Bauer, N.G., Richter-Landsberg, C. & Ffrench-Constant, C. Role of the oligodendroglial cytoskeleton in differentiation and myelination. *Glia* **57**, 1691–1705 (2009).

ONLINE METHODS

Mouse strains. *Plp1*-overexpressing transgenic mice[6] were the line 72 (PLP-tg$^{72/72}$, termed PMD mice) and the line 66 (PLP-tg$^{+/66}$) (**Supplementary Table 1**). Conditional *Fdft1* (farnesyl diphosphate farnesyl transferase gene 1 encoding squalene synthase, SQS)/*Cnp*-cre mice (mutants *Fdft1*$^{flox/flox}$ × *Cnp1*$^{+/cre}$ and controls *Fdft1*$^{+/flox}$ × *Cnp1*$^{+/cre}$) have been described previously[5]. Mice received normal diet or the same diet containing 5% cholesterol (ssniff) *ad libitum*. Analyses were done using littermate mice of both sexes. All experiments were performed in compliance with and approved by the German Federal State of Lower Saxony.

Behavioral analyses. Motor coordination was assessed with a beam test. Mice were put on a beam (width 1.5 cm) and allowed to run toward a hiding box. Number of slips in a defined 55 cm distance were assessed (three repeats per time point). Visual acuity was assessed using a virtual-reality optomotor system[30] and performed as described[31]. Freely moving mice were exposed to moving sine-wave gratings of various spatial frequencies and contrasts. Mice reflexively track the gratings by head movements. The thresholds for grating acuity and contrast were measured at the following spatial frequencies: 0.031, 0.064, 0.092, 0.103, 0.192, 0.272 and 0.331 cycles per degree. Clinical score was determined as described[32].

Antibodies. β-actin (1:1,000, A3853 Sigma), GalC (1:500, galactocerebroside, MAB342 Chemicon), GFAP (1:300, Z0334 Dako), Lamp1 (1:1,000, 553792 Pharmingen), MAC3 (1:300, 553322 BD), MBP (1:300, A0623 Dako), PLP[33] (1:1,000), Septin7 (1:500, 18991 IBL), Strepavidin-Alexa488 (1:200, S11223 Invitrogen), WGA-Alexa594 (1:200, W11262 Invitrogen).

Histological and morphological analyses. After fixation with 4% paraformaldehyde, 4 µm of the optic nerve (between optic tract and retina) or cervical spinal cord were immunolabeled as described[5]. Evans blue (0.5 µg per g body weight), a fluorescent dye that binds albumin and stains neural tissue only in case of BBB disruption, was injected as 1% solution in PBS. After 4 h, mice were killed, and Evans blue–derived fluorescence was visualized in frozen brain sections. Specimens were analyzed by light microscopy (Zeiss Axiophot, Zeiss Axio Imager.Z1 with ApoTome or using a confocal laser scanning microscope, Leica DM RXA). Images were processed by using US National Institutes of Health ImageJ software. BODIPY-cholesterol (Avanti Polar Lipids), a fluorescent derivative biochemically and biophysically similar to cholesterol[34], was injected i.p. (16 µg per g body weight). After 7 d, BODIPY-cholesterol was visualized in the perfusion-fixed optic nerve by a custom-made two-photon laser scanning microscope equipped with a femtosecond-pulsed titanium-sapphire laser (Chameleon Vision II; Coherent) and a Zeiss W Plan Apochromat 20× (NA 1.0) water immersion objective. Z-stacks of maximal 100-µm depth were obtained and processed to maximum intensity projections. Ultrastructural analysis and immunolabeling on ultrathin cryosections were done as described[5,35]. Oligodendrocytes in optic nerve sections were identified and counted on methylene blue/Azur II–stained resin sections on the basis of their characteristic morphology, such as dark cytoplasm, morphology of processes and shape of nucleus. Identification of oligodendrocytes was confirmed by electron microscopy showing characteristic short cisternae of granular endoplasmic reticulum. G-ratio analysis to quantify myelin content over axon caliber was done as described[21] with the ratio of fiber diameter divided by axon diameter taken as correlate for myelin thickness.

Biochemical analyses. Western blotting was done according to standard procedures[5]. Expression and purification of BCθ was done as described[23], followed by BCθ biotinylation (RPN 2202 GE Healthcare).

Cell culture. Primary oligodendrocytes were prepared as described[5] or using the P3 Oligodendrocyte Isolation Kit (P.Glia). Cholesterol was added from ethanolic stock solution at 10 µg ml^{-1}. Zaragozic acid (Sigma) was added after 1 d *in vitro* at 2 µM. Immunocytochemistry was performed using standard procedures[21]. Briefly, fixed cells (10 min, 4% paraformaldehyde) were permeabilized with 0.1% Triton X-100 for 5 min, blocked (30 min in blocking solution 2% BSA in PBS). Primary antibodies diluted in blocking solution were applied overnight at 4 °C. After washing with PBS, cells were incubated with secondary antibodies in blocking solution containing 0.2 µg ml^{-1} DAPI or 50 µg ml^{-1} filipin (Sigma) for 1 h. Quantification of filipin-derived fluorescence was done as previously described[22]. After selecting the soma area of the cell, the mean intensity of cellular filipin-derived fluorescence was measured. Live cell staining was done as described[21]. Biotinylated BCθ was used as previously described[36] at 0.015 mg ml^{-1} and visualized with streptavidin-coupled Alexa488 (Invitrogen). For quantification, the mean fluorescence intensity was measured in the surface area that was determined by colabeling with wheat germ agglutinase (WGA) or colabeling for GalC.

Quantitative PCR. Quantitative real-time RT-PCR was done as previously described[5]. RT-PCR primers were specific for β-actin (5′-CTTCCTCCC TGGAGAAGAGC and 5′-ATGCCACAGGATTCCATACC), *Apc* (5′-TTCT AGCGGCACGCACTCT and 5′-CGTGACATATCGTCCTTATCATGAG), cyclophilin (5′-ACCCCACCGTGTTCTTCGA and 5′- CATTTGCCATGG ACAAGATG), *Fdft1* (5′-ATCAGACCAGTCGCAGCTTT and 5′-CGGAGA ACCAGGTCGAACACA), *Hmgcr* (5′-TGATTGGAGTTGGCACCAT and 5′-TGGCCAACACTGACATGC), *Mbp* (5′-GCCTCCGTAGCCAAATCC and 5′-GCCTGTCCCTCAGCAGATT) or *Plp1* (5′-GGCTAGGACATCCCGACAAG and 5′-GCAAACACCAGGACCATACA).

Statistical analysis. All numerical values are shown as the mean ± s.e.m.; $n = 3–9$, unless stated otherwise. Statistical significance was determined by the Student's *t* test or by one- or two-way analysis of variance (ANOVA) followed by Bonferroni's test. In the case of clinical score analysis, the nonparametric Mann-Whitney test was applied.

30. Prusky, G.T., Alam, N.M., Beekman, S. & Douglas, R.M. Rapid quantification of adult and developing mouse spatial vision using a virtual optomotor system. *Invest. Ophthalmol. Vis. Sci.* **45**, 4611–4616 (2004).
31. Goetze, B. *et al.* Vision and visual cortical maps in mice with a photoreceptor synaptopathy: reduced but robust visual capabilities in the absence of synaptic ribbons. *Neuroimage* **49**, 1622–1631 (2010).
32. Stromnes, I.M. & Goverman, J.M. Active induction of experimental allergic encephalomyelitis. *Nat. Protoc.* **1**, 1810–1819 (2006).
33. Jung, M., Sommer, I., Schachner, M. & Nave, K.A. Monoclonal antibody O10 defines a conformationally sensitive cell-surface epitope of proteolipid protein (PLP): evidence that PLP misfolding underlies dysmyelination in mutant mice. *J. Neurosci.* **16**, 7920–7929 (1996).
34. Hölttä-Vuori, M. *et al.* BODIPY-cholesterol: a new tool to visualize sterol trafficking in living cells and organisms. *Traffic* **9**, 1839–1849 (2008).
35. Möbius, W. *et al.* Immunoelectron microscopic localization of cholesterol using biotinylated and non-cytolytic perfringolysin O. *J. Histochem. Cytochem.* **50**, 43–55 (2002).
36. Waheed, A.A. *et al.* Selective binding of perfringolysin O derivative to cholesterol-rich membrane microdomains (rafts). *Proc. Natl. Acad. Sci. USA* **98**, 4926–4931 (2001).

doi:10.1038/nm.2833